

# Molecular thermal engine based on a highly flexible elastic crystal

Hinako Kato,<sup>a</sup> Yoji Horii<sup>a\*</sup>, Chiharu Watanabe<sup>a</sup>, Toshiyuki Sasaki<sup>b</sup>, Kouhei Ichiiyanagi<sup>b</sup>, Mariko Noguchi<sup>c</sup>, Hiroki Fujimori<sup>c</sup>, Taro Yamamoto<sup>d</sup>, Hal Suzuki<sup>d</sup>, Yuichi Hirai<sup>e</sup>, Takahito Ohmura<sup>e</sup>, Keigo Yano<sup>f</sup>, Shotaro Hayashi<sup>f,g</sup>, and Takashi Kajiwara<sup>a</sup>

## Affiliations

*a. Graduate School of Humanity and Science, Nara Women's University, Kitauoya-Higashimachi, Nara 630-8506, Japan*

*b. SPring-8/JASRI, Kouto, Sayo, Hyogo 679-5198, Japan*

*c. Graduate School of Integrated Basic Sciences, Nihon University, 3-25-40 Sakurajosui, Setagaya-ku, Tokyo 156-8550, Japan*

*d. Department of Chemistry, Kindai University, 3-4-1 Kowakae, Higashiosaka City, Osaka 577-8502, Japan*

*e. National Institute for Materials Science (NIMS), 1-1 Namiki, Tsukuba, Japan*

*f. School of Engineering Science, Kochi University of Technology, 185 Miyanokuchi, Tosayamada, Kami, Kochi 782-8502, Japan*

*g. FOREST Center, Research Institute, Kochi University of Technology, 185 Miyanokuchi, Tosayamada, Kami, Kochi 782-8502, Japan*

## Abstract

Materials that exhibit actuation behavior in response to external stimuli have a wide range of applications owing to their ability to convert input energy into mechanical work. Light and chemicals are common sources of input energy. However, actuation using thermal energy from ambient-temperature sources remains challenging. In this study, we introduce novel elastic crystals composed of dodecylated porphyrin molecules that exhibit high flexibility and deformation in response to temperature changes. When a crystal is loaded with a small weight and positioned between high- and low-temperature heat sources, it exhibited continuous, large, and rapid oscillations. These oscillations persisted for at least 160 h, corresponding to 3.9 million deformation cycles, as long as the temperature difference was maintained. This study presents the first example of a molecular crystal functioning as an engine that can extract kinetic energy from static and ambient-temperature sources.

## INTRODUCTION

Materials exhibiting actuation properties in response to external stimuli have been extensively studied owing to their wide range of applications, including soft robotics, the medical industry (artificial muscles and limbs), and energy storage and conversion. Sophisticated material design has led to the development of soft polymer composites exhibiting autonomous locomotion similar to that of living organisms.<sup>1–9</sup> Liquid crystal elastomers exhibit continuous rolling<sup>10,11</sup> and oscillation<sup>4,7,9,12</sup> when exposed to consistent light and temperature. In these examples, mechanical energy is extracted from a nearly constant external field, eliminating the need for on–off cycling of the light or heat source. Typically, light serves as the energy source, inducing localized expansion and contraction either through the *E-Z* isomerization of photoresponsive molecules or via photothermal heating. These spatially non-uniform deformations disrupt symmetry and generate directional motions such as oscillation and locomotion. In many cases, asymmetry is maintained by self-shadowing effects, in which light-induced deformation dynamically alters the material geometry or orientation, thereby modulating its exposure to incident light. This spatiotemporal feedback mechanism enables a continuous and self-sustained motion under continuous illumination.

Recent developments in crystal engineering have revealed the possibility of endowing organic crystals, which were previously considered rigid, with actuation properties.<sup>13–24</sup> Elastic crystals that can be reversibly bent like elastomers while maintaining their crystallinity have also been reported;<sup>25</sup> these materials are considered promising materials for highly durable and flexible optoelectronic<sup>26–32</sup> and magnetic devices.<sup>33–36</sup> Reports on elastic crystals exhibiting actuation in response to light,<sup>37–39</sup> chemicals,<sup>40</sup> and temperature<sup>23,41,42</sup> underscore the diversity of the operating principles of actuators prepared from molecular crystals. Polymer composites containing highly oriented microcrystals grown epitaxially exhibit excellent photomechanical performance,<sup>43</sup> highlighting the importance of well-aligned molecular units in generating strong actuation forces through the accumulation of subtle molecular structural changes. In this context, crystals with highly ordered and oriented molecular packing are promising candidates for high-performance actuators. However, energy extraction from a constant external field, as demonstrated in polymer composites, remains rare in organic crystals.<sup>17</sup> Some molecular crystalline materials composed of photoresponsive molecules have exhibited continuous oscillations<sup>21,44</sup> and rolling<sup>45</sup> motions under steady light exposure, driven by self-shadowing effects similar to those observed in soft polymer systems. In contrast, while thermally induced actuation has been demonstrated in crystals, these systems typically rely on fluctuating external conditions, such as heater on-off cycling, to sustain

motion.<sup>18–20,22–24,39,46</sup> Therefore, the direct extraction of kinetic energy from static thermal baths, as in a thermal engine, remains an unresolved challenge. To address the gaps in the literature, in this study, we present the first example of a thermal engine based on elastic crystals. When the crystal is loaded with a weight and placed between high (34–37 °C)- and low (~0 °C)-temperature heat sources, it continuously oscillates, indicating that it can extract the kinetic energy from the heat sources at different temperatures. The oscillations continued for at least 160 h, corresponding to over 3.9 million cycles of bending and stretching, demonstrating the high durability of the elastic crystal. To the best of our knowledge, this study is the first to report the continuous operation of an organic crystal-based thermal engine under only static temperature differences. Our results highlight the potential applications of organic elastic crystals as actuators owing to their high-speed responsiveness to external fields and remarkable durability.

## RESULTS & DISCUSSION

### Synthesis and characterization

The dodecylated porphyrin molecule was synthesized by the ester-exchange reaction of 10,15,20-tetrakis(4-methoxycarbonylphenyl) porphyrin  $H_2$ (TMCPP) in 1-dodecanol in the presence of a base catalyst (DBU), as depicted in Figure 1a.<sup>36</sup> Crystallization of the deacylated porphyrin using dichloromethane and ethanol at 40 °C afforded the needle-like elastic crystals (**1**), with a minor amount of brittle block-shaped crystals (**2**). **1** could be bent under a mechanical force and returned to its original shape when the force is released, indicating its elasticity (Figure 1b and Movie 1). The nanoindentation test results for **1** (Figures S3 and S4) revealed a Young's modulus ( $E_r$ ) and hardness ( $H$ ) of 1.8(2) and 0.072(3) GPa, respectively. Furthermore, the Young's modulus of **1** upon bending was determined to be 0.13 GPa (Figures S5–S7). These values are lower than those of most organic compounds<sup>47</sup>, confirming the high flexibility of **1**.



**Figure 1.** (a) Synthesis and crystallization of dodecylated porphyrin. (b) Bending of **1**.

Figure 2a summarizes the crystal packing of **1** at 298 K. **1** crystallized in the space group  $P-1$ , and the entire molecule was crystallographically independent. The two dodecyl chains of **1** exhibited

heavy disorder at 298 K, as indicated in green, orange, and purple. The porphyrin molecules stacked along the *a*-axis to form a columnar structure surrounded by dodecyl chains. The *a*-axis coincided with the direction of crystal growth. Needle-like crystals with such a one-dimensional molecular arrangement are commonly elastic.<sup>26,48</sup> The intracolumnar distances between porphyrin  $\pi$ -planes (3.67 and 3.82 Å) are longer than that expected for a  $\pi$ - $\pi$  stacked system (3.3 Å), indicating that the van der Waals interactions between dodecyl chains are the dominant driving force behind the one-dimensional packing of the crystals. The brittle crystal **2** exhibits a complex packing structure in which the dodecyl chains are intricately intertwined (Figure S8), thereby restricting molecular displacement during bending. Energy framework analysis<sup>49</sup> revealed that in crystal **1**, the strongest intermolecular interactions are oriented along the *a*-axis, consistent with its one-dimensional columnar packing (Figure S10). In contrast, crystal **2** exhibits two similarly strong intermolecular interactions within a plane, reflecting its two-dimensional packing motif (Figure S11).

Figure 2b summarizes the temperature dependence of the *a*-axis length as a representative parameter. When the temperature was swept from approximately 275 to 223 K, the *a*-axis length gradually increased with the gradual suppression of the disorder on the dodecyl chains (Figure 2c). The crystalline parameters exhibited a similar temperature dependence during the corresponding heating process, indicating that this process is reversible. Adiabatic and differential scanning calorimetry indicated that the gradual structural changes observed between 275 and 223 K correspond to a second- or higher-order phase transition from the high-temperature (HT) to the low-temperature (LT) phase (see the thermal analysis section in the Supporting Information (SI)). In this paper, the 275–223 K region is referred to as the medium-temperature (MT) state for convenience. The *a*-axis length of **1** increases with decreasing temperature, whereas its *b*-axis length, *c*-axis length, and cell volume decrease. In other words, the needle-like crystals become long and slim upon cooling. The elongation ratio of the crystals associated with the decrease in temperature was observed using optical microscopy (Figure S12 and Table S3). The increase in *a*-axis length correlated with the magnitude of disorder of the dodecyl groups. The heavy thermal motion of the dodecyl chains in the HT phase prevented the porphyrin columns from approaching each other, whereas the suppressed thermal motion of the dodecyl chains upon cooling decreased the intercolumnar distances (Figure 2d). Owing to the chemical pressure from adjacent columns, the intracolumnar molecular distances increased, resulting in an increase in *a*-axis length.

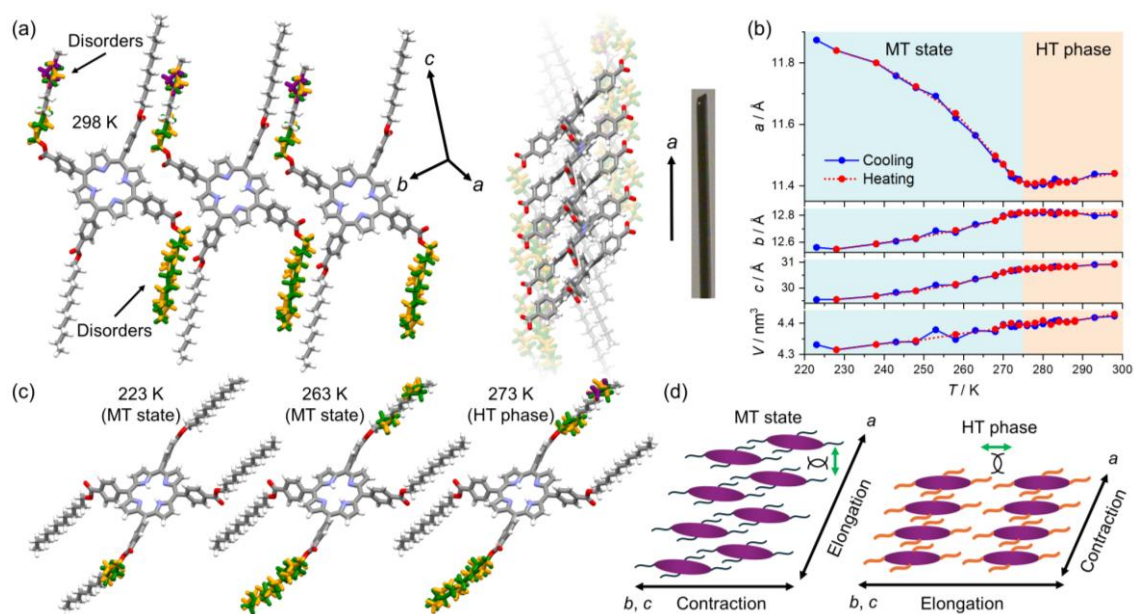


**Figure 2.** (a) X-ray structures of **1** at 298 K. (b) Temperature dependence of the crystal parameters and (c) X-ray structures of **1**. (d) Schematic illustration of the elongation of the *a*-axis and contraction of the *b*- and *c*-axes upon cooling.

### Crystal deformation by changes in temperature

An important consideration in the performance of elastic crystals is their ability to remain flexible at low temperatures.<sup>50,51</sup> Because **1** contains dodecyl chains that exhibit temperature-dependent thermal motion, its flexibility should depend on the temperature. To briefly examine the temperature dependence of the flexibility of **1**, we attached a weight (1.168 mg of Al) to the tip of **1** (length: 5.7 mm) and cooled the crystal in a refrigerant-free cooling device sealed with an insulated window.<sup>36</sup> Figure 3a summarizes the deformation of the crystal with the weight load upon cooling and heating (Movie 2). Surprisingly, the crystal bent during cooling from 298 to 265 K, indicating that the crystal softens as the temperature decreases. This behavior is unusual because typical solids harden with decreasing temperature. A further decrease in temperature from 265 to 251 K straightened the crystal owing to curing. The heating process induced a crystal deformation identical to that observed during the cooling process, indicating that the deformation of the crystal with changing temperature is reversible.

Notably, in the absence of an applied weight, the crystal exhibited only a change in length while retaining a straight configuration without any bending deformation (Figure S12). This observation indicates that the mechanical stress generated by the attached weight is essential for inducing the bending behavior.

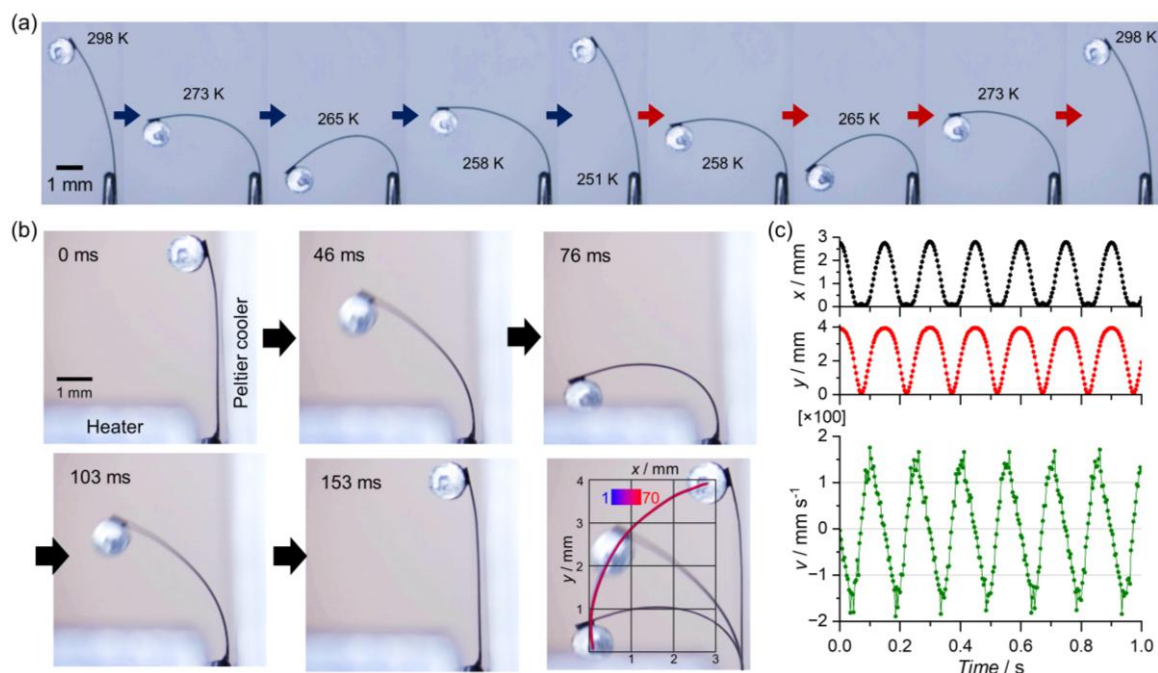


**Figure 3.** (a) Temperature-dependent deformation of **1** with a weight load. (b) Movement of the weight during the thermal-engine experiments. The track of the weight over 70 cycles of oscillation is depicted as a solid curve. (c) Time dependence of the  $x$  coordinate,  $y$  coordinate, and velocity ( $v$ ) of **1** over 1 s.

### Construction of the thermal engine

When **1** is loaded with a weight (1.168 mg of Al) and sandwiched between a high-temperature (34–37 °C) heat source and a low-temperature ( $\sim 0$  °C) heat source, a thermal engine that can extract kinetic energy from thermal energy is constructed. The crystal is  $\sim 5.2$  mm long and  $\sim 43$   $\mu\text{m}$  thick (Figure S18). As shown in Figure 3b, the weight attached to the crystal moves with a large oscillation at a frequency of 6.84(7) Hz. When the Peltier cooler is switched on, the crystal begins to vibrate, and the vibrations are gradually amplified until a large oscillating motion is achieved (Movie 3). This movement continues as long as the temperatures of the heat sources are maintained, and was confirmed to last for at least 160 h, corresponding to over 3.9 million cycles of bending and stretching. Unlike a previous example of molecular crystals that could extract kinetic energy from heat,<sup>19</sup> our crystal does not require periodic changes in temperature for actuation. Thus, to the best of our knowledge, our molecular crystal-based heat engine is the first of its kind. Figures 3c and S21 summarize the time dependence of the  $x$  and  $y$  coordinates as well as the velocity ( $v$ ) of the weight, clearly demonstrating the high reversibility of the lifting and descending cycles (Movie 4). The average time interval for the descending and lifting processes over 70 cycles was 0.146(1) s. The maximum  $v$  ( $v_{\text{max}}$ ) of the weight was 174(9)  $\text{mm s}^{-1}$  for

descending and 179(14) mm s<sup>-1</sup> for lifting (Figure S23); these values are 5–6 times faster than the reported  $v$  of a glass bead (0.15 mg) pushed by a thermoelastic organic crystal (29 mm s<sup>-1</sup>).<sup>39</sup>

Figure 4a summarizes the thermodynamic cycle of the heat engine. As the crystal approaches the low-temperature heat source (273 K; state A), it deforms from its equilibrium position by  $\Delta q = \sim 5$  mm (state B and Figure S19) owing to bending. Using an elastic constant  $k$  of 2.94 mN m<sup>-1</sup> (as summarized in Figure S20), we determined the elastic energy ( $E_{\text{El}}$ ) to be  $k(\Delta q)^2/2 = 37$  nJ.  $k$  rapidly increased to 5.48 mN m<sup>-1</sup> when **1** was heated by the high-temperature heat source (298 K; state C), and  $E_{\text{El}}$  increased to 69 nJ. In other words, 32 nJ of  $E_{\text{El}}$  was supplied from the thermal energy. Based on the  $v$  and  $y$  (height) of the weight, the time dependence of its kinetic energy ( $E_{\text{K}}$ ) and potential energy owing to gravity ( $E_{\text{G}}$ ) can be calculated as  $mv^2/2$  and  $mgy$ , respectively, where  $g$  is the gravitational acceleration and  $m$  is the mass of the weight. Figure 4b summarizes  $E_{\text{El}}$ ,  $E_{\text{G}}$ ,  $E_{\text{K}}$ , and their sum ( $E_{\text{T}}$ ). The maximum  $E_{\text{El}}$  ( $\sim 69$  nJ) is greater than the maximum  $E_{\text{G}}$  ( $\sim 45$  nJ), indicating that the  $E_{\text{El}}$  stored via the temperature change is sufficient to lift the weight to its highest position ( $y = \sim 3.8$  mm). In other words, the  $E_{\text{El}}$  supplied from the heat source is sufficiently large for the fast and continuous motion of the weight. Based on the thermal energy absorbed by **1** as the temperature is increased from 273 to 298 K (1.0 mJ, as summarized in the caption of Figure S18) and the supplied  $E_{\text{El}}$  (32 nJ), the energy conversion efficiency of our system was estimated to be 0.003%, which is similar to that of a photothermally driven crystal actuator.<sup>39</sup> The work density (output energy of 32 nJ per volume of 0.031 mm<sup>3</sup>) was estimated to be approximately 1 kJ m<sup>-3</sup>, which falls within the range reported for crystal-based actuators.<sup>24,52,53</sup> This heat-engine behavior is highly reproducible, and large vibrations could be observed even in crystals of low quality (bent or chipped) (Figures S25–S27 and Movies 5–8). The oscillatory engine behavior is not observed in the absence of an attached weight, as bending deformation does not occur under such conditions. Furthermore, the magnitude of the attached weight is a critical factor in achieving large amplitude oscillations. If the weight is too light, the resulting stress is insufficient to induce the necessary bending, preventing the cooled crystal from reaching the high-temperature source. Conversely, if the weight is too large, the crystal cannot lift it, thereby inhibiting the approach to the low-temperature source. The optimal weight depends on the dimensions of the crystal. A longer crystal requires a smaller weight to deform effectively due to the larger moment arm, making them well-suited for generating significant oscillations under lighter loads. In contrast, thicker crystals exhibit greater stiffness, and therefore require heavier weights to induce sufficient bending and generate pronounced oscillatory motion. In addition to enabling deformation, the attached weight also serves to store kinetic energy ( $E_{\text{K}}$ ) through its inertia, assisting the crystal in

traveling back and forth between the low- and high-temperature heat sources—similar to the function of a flywheel in conventional thermal engines. In addition, to maximize the oscillation amplitude, the heater and cooler should be positioned as close as possible without contacting the crystal during its motion.

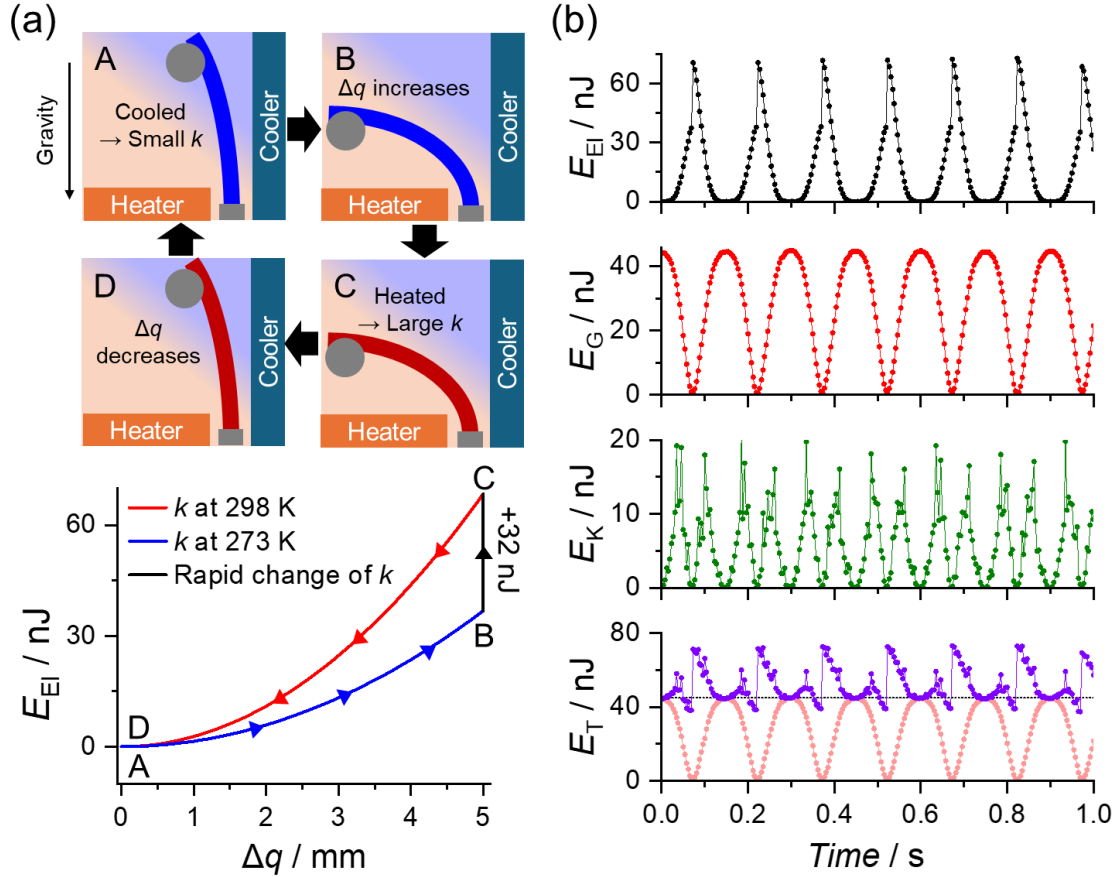


**Figure 4.** (a) Thermal cycle of the heat engine. (b) Time dependence of the energies of the heat engine. The potential energy owing to gravity ( $E_G$ ) and maximum  $E_G$  (45 nJ) are shown in the total energy ( $E_T$ ) vs. time plot as red curves and black dotted line for comparison.  $E_K$  = kinetic energy,  $E_{El}$  = elastic energy.

### Microscopic mechanism of bending upon cooling

The thermal-engine behavior of **1** is driven by changes in  $k$  with temperature. Notably, the temperature at which the crystal becomes most bendable (265 K in Figure 3a) is close to the boundary between the HT phase and MT state ( $\sim 270$  K in Figure 2b), indicating that bending is correlated with its structural changes. The following bending mechanism can be proposed based on the elongation of the crystal upon cooling (Figure 5a). (1) The weight causes the elastic crystal to arc. The outer arc is stretched, whereas the inner arc is compressed. That is, the mechanical



force elongates the  $a$ -axis in the outer arc and compresses the  $a$ -axis in the inner arc. (2) When the crystal is cooled to approximately 270 K, the outer-arc region preferentially changes to the MT state with a preference for a long  $a$ -axis, whereas the inner-arc region remains in the HT phase with a preference for a short  $a$ -axis. Such an inhomogeneous structural phase transition renders the outer arc longer and the inner arc shorter, resulting in the bending of the crystal upon cooling. During this process, part of the potential energy from the attached weight is used to maintain the energetically unfavorable HT phase in the inner arc, thereby stabilizing the curved configuration. (3) Further decreases in temperature convert the crystal into an entirely MT state, causing it to straighten (251 K in Figure 3a). At this stage, the portion of the enthalpy released from the HT-to-MT phase transition (estimated to be on the order of  $10^{-4}$  J) is partially utilized to lift the weight, which requires only  $\sim 10^{-8}$  J of gravitational potential energy. The bending mechanism proposed here is identical to the operating principle of bimetals, and a similar type of curing by decreases in temperature has been reported for composite materials composed of elastic crystals, metals, and polymers.<sup>31</sup>

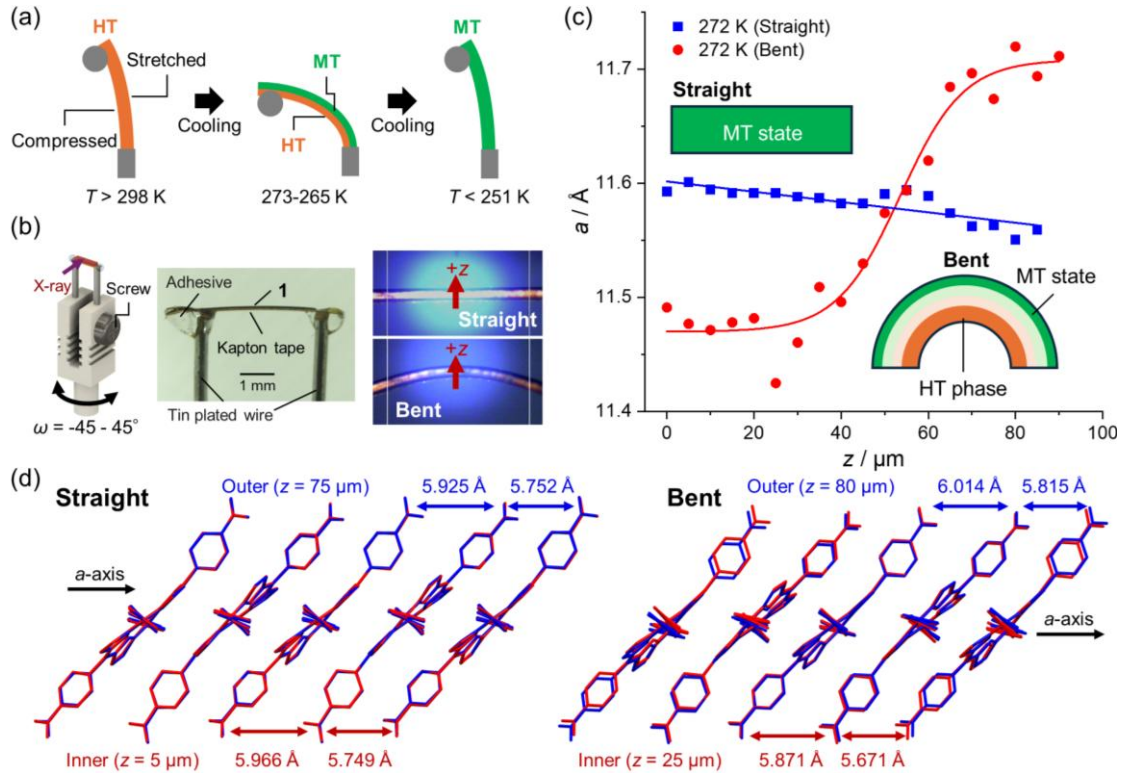


**Figure 5.** (a) Mechanism of the bending of the crystal based on the elongation of the  $a$ -axis upon cooling. (b) Experimental setup for the pinpoint X-ray structural measurements. (c) Variation in  $a$ -axis length as a function of the  $z$  position along the crystal. The solid lines represent the fits obtained using linear and

sigmoidal equations. (d) Crystal structures for the inner (small  $z$ )- and outer (large  $z$ )-arc regions in the straight (left) and bent (right) configurations. The intermolecular centroid–centroid distances are shown for comparison.

To confirm the inhomogeneous structural phase transition of the crystal arc near the phase-transition temperature, we performed pinpoint X-ray structural analyses<sup>54</sup> of the crystal arc. Based on the crystal mount pin used to stretch crystals<sup>55</sup> reported by Shi *et al.*, we created a 3D model of a mount pin that could bend the crystal by adjusting a screw (Figure 5b and 3D data in the SI). The crystal was adhered to a rectangular piece of Kapton tape to prevent it from moving and fluctuating under the N<sub>2</sub> gas stream used for temperature control. The crystal had a straight configuration before the screw was tightened. The position of the microfocus X-ray beam (height: 2  $\mu\text{m}$ ; width: 4  $\mu\text{m}$ ) was moved from the top to the bottom of the linear crystal to scan its local structure. The  $\omega$ -scan range was restricted to  $-45^\circ$  to  $45^\circ$  to avoid the X-ray irradiation of positions other than the center of the crystal. As summarized in Figure 5c, the  $a$ -axis length of the straight crystal was nearly independent of the beam position and similar to that in the MT state. Tightening of the screw caused the crystal to arc. Structural mapping from the lower to the upper regions across the center of the arc revealed that the  $a$ -axis length of the outer arc was approximately 1.7% longer than that of the inner arc. The longer and shorter  $a$ -axis lengths correspond to the MT state and HT phase, respectively, indicating that the outer- and inner-arc regions adopt the MT state and HT phase, respectively. The  $z$  dependence of the  $a$ -axis length of a bent crystal is not expressed as a linear line<sup>33,56</sup> but is fitted with a sigmoidal curve, indicating an inhomogeneous structural phase transition. These results are consistent with the proposed mechanism of bending upon cooling, where the outer- and inner-arc regions adopt the MT state and HT phase, respectively (Figure 5a).

Figure 5d summarizes the porphyrin core structures in the inner (small  $z$ )- and outer (large  $z$ )-arc regions. The molecular structures of the outer- and inner-arc regions of the straight and bent configurations were identical, and no clear difference in the magnitudes of the thermal factors on the dodecyl chains was observed. In contrast to the molecular structures, the intracolumnar molecular distances depended on the position of the arc. In the straight configuration, the intermolecular centroid–centroid distances in the outer- and inner-arc regions were similar (Figure 5d, left). However, in the bent configuration, the intermolecular distances changed from 5.87 to 6.01 Å in the inner arc and from 5.67 to 5.81 Å in the outer arc, corresponding to a  $\sim 2.3\%$  difference in molecular distance (Figure 5d, right). This deformation indicates that a 60  $\mu\text{m}$ -thick crystal can be bent to form an arc with a diameter of 5.2 mm, indicating high flexibility.

## CONCLUSION

We successfully constructed a molecular crystal-based thermal engine that can extract kinetic energy from ambient-temperature differences. The flexible conversion of the kinetic energy of the weight to the potential energy of crystal deformation and the rapid deformation of the crystal to accelerate the weight are crucial factors for continuous motion. The bending of the weight-loaded crystal as the temperature decreases correlates with the strain-induced phase transition associated with crystal elongation, which occurs preferentially in the outer-arc region. The mechanical properties and energy efficiency of our porphyrin-based system can be modified by changing the alkyl chain length, inserting metals, and constructing solid solutions. The direct conversion of ambient temperature differences into kinetic energy, as demonstrated here, opens up new possibilities for applying organic crystals in waste-heat utilization.

## METHODS

### Synthesis of **1**

The mixture of H<sub>2</sub>(TMCPP) (110 mg, 0.13 mmol), 1-dodecanol (2 mL) and DBU (80  $\mu$ L) was stirred at 180 °C for 12 hours under N<sub>2</sub> atmosphere. After cooling to room temperature, the excess methanol (ca. 30 mL) was added to the reaction mixture to afford the precipitate, which was collected by vacuum filtration and washed with methanol. The precipitate was purified with the silica gel column chromatography (Wakogel 60N) with CH<sub>2</sub>Cl<sub>2</sub> as the eluent. Recrystallization using CH<sub>2</sub>Cl<sub>2</sub> and ethanol afforded purplish red crystals of **1** (84 mg, 65 %). Crystallization using CH<sub>2</sub>Cl<sub>2</sub> and ethanol at 40 °C afforded the needle crystals of **1**. <sup>1</sup>H NMR (400 MHz, CDCl<sub>3</sub>, TMS):  $\delta$  8.214 (s, 8H), 8.45 (d, 8H), 8.29 (d, 8H), 4.51 (t, 8H), 1.92 (quint., 8H), 1.28 (broad signal, 72H), 0.86 (t, 12H), -2.803 (s, 2H). MALDI-TOF MS (Matrix: HABA): Calcd. for [C<sub>96</sub>H<sub>126</sub>N<sub>4</sub>O<sub>8</sub>]<sup>+</sup>:  $m/z$  = 1483.96. Found: 1483.87. CHN elemental analysis calcd. (%) for C<sub>96</sub>H<sub>126</sub>N<sub>4</sub>O<sub>8</sub>: C 78.76, H 8.67, N 3.83; found: C 78.569, H 8.671, N 3.77. Melting point: 422-426 K.

### Pinpoint X-ray structural analyses

Pinpoint X-ray structural analyses were performed on SPring-8 BL40XU using the mount pin printed by 3D printer. The diffraction data was processed via CrysAlisPro 4.0. Initial structures were determined using SHELXT (2018/3) and subsequently refined with SHELXL (2018/3)<sup>57</sup>, in combination with Yadokari-XG.<sup>58</sup>

### Mechanical testing

Stress-strain curve of a crystal was evaluated using automatic cantilever bending instrument.<sup>47</sup> Small loads were applied in the direction perpendicular to the mounted needle crystals using a KYOWA LTS 50GA ultra-small-capacity load cell. The crystals were fixed on the slide glass with an araldite adhesive. The stress ( $\sigma$ ), strain ( $\epsilon$ ) and Young's modulus ( $E$ ) in a cantilever bending can be calculated by Figure S5. Nanoindentation test was performed on Triboindenter system (Hysitron Inc. Triboindenter TI950) equipped with a 60° 3-sided pyramidal tip on fused quartz (Hysitron Inc. Ti-0038).

### **Thermal engine experiments**

Movies of the crystal during thermal engine experiment were captured using an ELP-USBFHD08s-MFV(5-50) camera with a HAYEAR C-Mount lens (0.7–4.5x) and a HAYEAR LED ring light. High-speed footage (260 fps) was recorded with AMCap software, while other videos were captured using OBS Studio. The trajectory of the weigh was obtained by Kinovea software.<sup>59</sup>

### **Acknowledgement**

This work was supported by JSPS KAKENHI grants JP23K04875 (Y.H.), JP21K14645 (Y.H.), JP20K15293 (T.K.), and JP22K14661 (Y.H.<sup>o</sup>). Y.H. acknowledges the financial support of The Mazda Foundation (2024). The X-ray pinpoint structural diffraction measurements were performed at the BL40XU beamline at SPring-8 (2024A1219 and 2024B1168). Y.H. thanks Prof. Takashi Nakazawa (Nara Women's University) for assisting in the MALDI-TOF MS measurements and Ms. Chihiro Kondo (Nara Prefectural Institute of Industrial Development) for assisting in the nanoindentation measurements.

### **Author contributions**

All authors have given approval to the final version of the manuscript.

### **Notes**

The authors declare no competing interests.

### **Supporting information**

**PDF:** Structural and mechanical characterization data

**Movie 1:** Reversible bending of the crystal

**Movie 2:** Temperature-dependent deformation of the crystal under applied load

**Movie 3:** Thermal engine behavior of the crystal

**Movie 4:** Slow-motion video of the thermal engine

**Movie 5:** Thermal engine behavior of sample 1

**Movie 6:** Thermal engine behavior of sample 2

**Movie 7:** Thermal engine behavior of sample 3

**Movie 8:** Thermal engine behavior of sample 4

**Movie 9:** Collapse of the crystal during heating and cooling between 20 and  $-120\text{ }^{\circ}\text{C}$

**Track.xlsx:** Time-dependent trajectory of the weights in the thermal engine experiments

**3D\_data\_for\_printing.zip:** 3D model files for the crystal mount pin and thermal engine apparatus

### Author Information

Corresponding Author

Yoji Horii, Graduate School of Humanity and Science, Nara Women's University, Kitaouya-Higashimachi, Nara 630-8506, Japan

Present Address: Program in Advanced Materials Science, Faculty of Engineering and Design, Kagawa University, 2217-20 Hayashi-cho, Takamatsu, Kagawa 761-0396, Japan

Email: [horii.yoji@kagawa-u.ac.jp](mailto:horii.yoji@kagawa-u.ac.jp)

### References

- (1) Camacho-Lopez, M.; Finkelmann, H.; Palffy-Muhoray, P.; Shelley, M. Fast Liquid-Crystal Elastomer Swims into the Dark. *Nat. Mater.* **2004**, *3* (5), 307–310.
- (2) Maeda, S.; Hara, Y.; Sakai, T.; Yoshida, R.; Hashimoto, S. Self - walking Gel. *Adv. Mater.* **2007**, *19* (21), 3480–3484.
- (3) Yamada, M.; Kondo, M.; Mamiya, J.-I.; Yu, Y.; Kinoshita, M.; Barrett, C. J.; Ikeda, T. Photomobile Polymer Materials: Towards Light-Driven Plastic Motors. *Angew. Chem. Int. Ed.* **2008**, *47* (27), 4986–4988.
- (4) White, T. J.; Tabiryan, N. V.; Serak, S. V.; Hrozhyk, U. A.; Tondiglia, V. P.; Koerner, H.; Vaia, R. A.; Bunning, T. J. A High Frequency Photodriven Polymer Oscillator. *Soft Matter* **2008**,

4 (9), 1796–1798.

- (5) Lee, K. M.; Smith, M. L.; Koerner, H.; Tabiryan, N.; Vaia, R. A.; Bunning, T. J.; White, T. J. Photodriven, Flexural-Torsional Oscillation of Glassy Azobenzene Liquid Crystal Polymer Networks. *Adv. Funct. Mater.* **2011**, *21* (15), 2913–2918.
- (6) Arazoe, H.; Miyajima, D.; Akaike, K.; Araoka, F.; Sato, E.; Hikima, T.; Kawamoto, M.; Aida, T. An Autonomous Actuator Driven by Fluctuations in Ambient Humidity. *Nat. Mater.* **2016**, *15* (10), 1084–1089.
- (7) Gelebart, A. H.; Jan Mulder, D.; Varga, M.; Konya, A.; Vantomme, G.; Meijer, E. W.; Selinger, R. L. B.; Broer, D. J. Making Waves in a Photoactive Polymer Film. *Nature* **2017**, *546* (7660), 632–636.
- (8) Hu, W.; Lum, G. Z.; Mastrangeli, M.; Sitti, M. Small-Scale Soft-Bodied Robot with Multimodal Locomotion. *Nature* **2018**, *554* (7690), 81–85.
- (9) Zeng, H.; Lahikainen, M.; Liu, L.; Ahmed, Z.; Wani, O. M.; Wang, M.; Yang, H.; Priimagi, A. Light-Fuelled Freestyle Self-Oscillators. *Nat. Commun.* **2019**, *10* (1), 5057.
- (10) Wie, J. J.; Shankar, M. R.; White, T. J. Photomotility of Polymers. *Nat. Commun.* **2016**, *7* (1), 13260.
- (11) Ahn, C.; Li, K.; Cai, S. Light or Thermally Powered Autonomous Rolling of an Elastomer Rod. *ACS Appl. Mater. Interfaces* **2018**, *10* (30), 25689–25696.
- (12) Gelebart, A. H.; Vantomme, G.; Meijer, E. W.; Broer, D. J. Mastering the Photothermal Effect in Liquid Crystal Networks: A General Approach for Self-Sustained Mechanical Oscillators. *Adv. Mater.* **2017**, *29* (18), 1606712.
- (13) Kobatake, S.; Takami, S.; Muto, H.; Ishikawa, T.; Irie, M. Rapid and Reversible Shape Changes of Molecular Crystals on Photoirradiation. *Nature* **2007**, *446* (7137), 778–781.
- (14) Terao, F.; Morimoto, M.; Irie, M. Light-Driven Molecular-Crystal Actuators: Rapid and Reversible Bending of Rodlike Mixed Crystals of Diarylethene Derivatives. *Angew. Chem. Int. Ed.* **2012**, *51* (4), 901–904.
- (15) Kitagawa, D.; Nishi, H.; Kobatake, S. Photoinduced Twisting of a Photochromic Diarylethene Crystal. *Angew. Chem. Int. Ed.* **2013**, *52* (35), 9320–9322.
- (16) Karothu, D. P.; Weston, J.; Desta, I. T.; Naumov, P. Shape-Memory and Self-Healing Effects in Mechanosensitive Molecular Crystals. *J. Am. Chem. Soc.* **2016**, *138* (40), 13298–13306.
- (17) Ikegami, T.; Kageyama, Y.; Obara, K.; Takeda, S. Dissipative and Autonomous Square-Wave Self-Oscillation of a Macroscopic Hybrid Self-Assembly under Continuous Light Irradiation. *Angew. Chem. Int. Ed.* **2016**, *55* (29), 8239–8243.
- (18) Taniguchi, T.; Sugiyama, H.; Uekusa, H.; Shiro, M.; Asahi, T.; Koshima, H. Walking and Rolling of Crystals Induced Thermally by Phase Transition. *Nat. Commun.* **2018**, *9* (1), 538.
- (19) Duan, Y.; Semin, S.; Tinnemans, P.; Cuppen, H.; Xu, J.; Rasing, T. Robust Thermoelastic

- Microactuator Based on an Organic Molecular Crystal. *Nat. Commun.* **2019**, *10* (1), 4573.
- (20) Lin, J.; Guo, Z.; Zhang, K.; Zhao, P.; Wu, S.; Xu, J.; Gong, J.; Bao, Y. Mechanical Motion and Modulation of Thermal-Actuation Properties in a Robust Organic Molecular Crystal Actuator. *Adv. Funct. Mater.* **2022**, *32* (29), 2203004.
- (21) Lam, K.; Carta, V.; Almtiri, M.; Bushnak, I.; Islam, I.; Al-Kaysi, R. O.; Bardeen, C. J. Solar-Powered Molecular Crystal Motor Based on an Anthracene-Thiazolidinedione Photoisomerization Reaction. *J. Am. Chem. Soc.* **2024**, *146* (28), 18836–18840.
- (22) Uddin, M. A.; Martín, R.; Gámez-Valenzuela, S.; Echeverri, M.; Ruiz Delgado, M. C.; Gutiérrez Puebla, E.; Monge, A.; Gómez-Lor, B. Giant Thermosolient Effect in a Molecular Single Crystal: Dynamic Transformations and Mechanistic Insights. *J. Am. Chem. Soc.* **2024**, *146* (40), 27690–27700.
- (23) Wang, Z.; Cheng, P.; Han, W.; Shi, R.; Xu, J.; Zheng, Y.; Xu, J.; Bu, X.-H. Thermoelastic Twisting-Assisted Crystal Jumping Based on a Self-Healing Molecular Crystal. *Proc. Natl. Acad. Sci. U. S. A.* **2025**, *122* (7), e2417901122.
- (24) Wang, Z.; Shi, R.; Tahir, I.; Karothu, D. P.; Cheng, P.; Han, W.; Li, L.; Zheng, Y.; Naumov, P.; Xu, J.; Bu, X.-H. Thiophene Sulfone Single Crystal as a Reversible Thermoelastic Linear Actuator with an Extended Stroke and Second-Harmonic Generation Switching. *J. Am. Chem. Soc.* **2025**, *147* (9), 7749–7756.
- (25) Ghosh, S.; Reddy, C. M. Elastic and Bendable Caffeine Cocrystals: Implications for the Design of Flexible Organic Materials. *Angew. Chem. Int. Ed.* **2012**, *51* (41), 10319–10323.
- (26) Hayashi, S.; Koizumi, T. Elastic Organic Crystals of a Fluorescent  $\pi$ -Conjugated Molecule. *Angew. Chem. Int. Ed.* **2016**, *55* (8), 2701–2704.
- (27) Hayashi, S.; Yamamoto, S.-Y.; Takeuchi, D.; Ie, Y.; Takagi, K. Creating Elastic Organic Crystals of  $\pi$ -Conjugated Molecules with Bending Mechanofluorochromism and Flexible Optical Waveguide. *Angew. Chem. Int. Ed.* **2018**, *57* (52), 17002–17008.
- (28) Liu, H.; Lu, Z.; Zhang, Z.; Wang, Y.; Zhang, H. Highly Elastic Organic Crystals for Flexible Optical Waveguides. *Angew. Chem. Int. Ed.* **2018**, *57* (28), 8448–8452.
- (29) Kwon, T.; Koo, J. Y.; Choi, H. C. Highly Conducting and Flexible Radical Crystals. *Angew. Chem. Int. Ed.* **2020**, *59* (38), 16436–16439.
- (30) Chen, Y.; Chang, Z.; Zhang, J.; Gong, J. Bending for Better: Flexible Organic Single Crystals with Controllable Curvature and Curvature-Related Conductivity for Customized Electronic Devices. *Angew. Chem. Int. Ed.* **2021**, *60* (41), 22424–22431.
- (31) Yang, X.; Lan, L.; Pan, X.; Liu, X.; Song, Y.; Yang, X.; Dong, Q.; Li, L.; Naumov, P.; Zhang, H. Electrically Conductive Hybrid Organic Crystals as Flexible Optical Waveguides. *Nat. Commun.* **2022**, *13* (1), 7874.
- (32) Rohullah, M.; Pradeep, V. V.; Singh, S.; Chandrasekar, R. Mechanically Controlled

Multifaceted Dynamic Transformations in Twisted Organic Crystal Waveguides. *Nat. Commun.* **2024**, *15* (1), 4040.

- (33) Worthy, A.; Grosjean, A.; Pfrunder, M. C.; Xu, Y.; Yan, C.; Edwards, G.; Clegg, J. K.; McMurtrie, J. C. Atomic Resolution of Structural Changes in Elastic Crystals of Copper(II) Acetylacetonate. *Nat. Chem.* **2018**, *10* (1), 65–69.
- (34) Kenny, E. P.; Jacko, A. C.; Powell, B. J. Mechanomagnetism in Elastic Crystals: Insights from [Cu(Acac)<sub>2</sub>]. *Angew. Chem. Int. Ed.* **2019**, *58* (42), 15082–15088.
- (35) Yang, X.; Lan, L.; Li, L.; Liu, X.; Naumov, P.; Zhang, H. Remote and Precise Control over Morphology and Motion of Organic Crystals by Using Magnetic Field. *Nat. Commun.* **2022**, *13* (1), 2322.
- (36) Kato, H.; Horii, Y.; Noguchi, M.; Fujimori, H.; Kajiwar, T. Molecular Elastic Crystals Exhibiting Slow Magnetic Relaxations. *Chem. Commun. (Camb.)* **2023**, *59* (98), 14587–14590.
- (37) Hao, Y.; Gao, L.; Zhang, X.; Wei, R.; Wang, T.; Wang, N.; Huang, X.; Yu, H.; Hao, H. Azobenzene Crystal Polymorphism Enables Tunable Photoinduced Deformations, Mechanical Behaviors and Photoluminescence Properties. *J. Mater. Chem. C* **2021**, *9* (26), 8294–8301.
- (38) Peng, J.; Han, C.; Zhang, X.; Jia, J.; Bai, J.; Zhang, Q.; Wang, Y.; Xue, P. Mechanical Effects of Elastic Crystals Driven by Natural Sunlight and Force. *Angew. Chem. Int. Ed.* **2023**, *62* (48), e202311348.
- (39) Hagiwara, Y.; Hasebe, S.; Fujisawa, H.; Morikawa, J.; Asahi, T.; Koshima, H. Photothermally Induced Natural Vibration for Versatile and High-Speed Actuation of Crystals. *Nat. Commun.* **2023**, *14* (1), 1354.
- (40) Zheng, X.; Liu, X.; Liu, L.; Li, X.; Jiang, S.; Niu, C.; Xie, P.; Liu, G.; Cao, Z.; Ren, Y.; Qin, Y.; Wang, J. Multi-Stimuli-Induced Mechanical Bending and Reversible Fluorescence Switching in a Single Organic Crystal. *Angew. Chem. Int. Ed.* **2022**, *61* (1), e202113073.
- (41) Ghosh, S.; Mishra, M. K.; Ganguly, S.; Desiraju, G. R. Dual Stress and Thermally Driven Mechanical Properties of the Same Organic Crystal: 2,6-Dichlorobenzylidene-4-Fluoro-3-Nitroaniline. *J. Am. Chem. Soc.* **2015**, *137* (31), 9912–9921.
- (42) Hasija, A.; Ranjan, S.; Guerin, S.; Mangalampalli, S. R. N. K.; Takamizawa, S.; Chopra, D. Tracing Shape Memory Effect and Elastic Bending in a Conformationally Flexible Organic Salt. *J. Mater. Chem. C* **2022**, *10* (11), 4257–4267.
- (43) Xu, W.; Sanchez, D. M.; Raucci, U.; Zhou, H.; Dong, X.; Hu, M.; Bardeen, C. J.; Martinez, T. J.; Hayward, R. C. Photo-Actuators via Epitaxial Growth of Microcrystal Arrays in Polymer Membranes. *Nat. Mater.* **2023**, *22* (9), 1152–1159.
- (44) Tong, F.; Kitagawa, D.; Bushnak, I.; Al-Kaysi, R. O.; Bardeen, C. J. Light-Powered



- Autonomous Flagella-like Motion of Molecular Crystal Microwires. *Angew. Chem. Int. Ed.* **2021**, *60* (5), 2414–2423.
- (45) Bartholomew, A. K.; Stone, I. B.; Steigerwald, M. L.; Lambert, T. H.; Roy, X. Highly Twisted Azobenzene Ligand Causes Crystals to Continuously Roll in Sunlight. *J. Am. Chem. Soc.* **2022**, *144* (37), 16773–16777.
- (46) Hagiwara, Y.; Taniguchi, T.; Asahi, T.; Koshima, H. Crystal Actuator Based on a Thermal Phase Transition and Photothermal Effect. *J. Mater. Chem. C* **2020**, *8* (14), 4876–4884.
- (47) Hoshino, N.; Akutagawa, T. Large Electric Piezoresistance of the Flexible Molecular Semiconductive Crystal Q(TCNQ)<sub>2</sub> during Bending. *CrystEngComm* **2022**, *24* (29), 5234–5237.
- (48) Hayashi, S.; Ishiwari, F.; Fukushima, T.; Mikage, S.; Imamura, Y.; Tashiro, M.; Katouda, M. Anisotropic Poisson Effect and Deformation-Induced Fluorescence Change of Elastic 9,10-Dibromoanthracene Single Crystals. *Angew. Chem. Int. Ed.* **2020**, *59* (37), 16195–16201.
- (49) Spackman, P. R.; Turner, M. J.; McKinnon, J. J.; Wolff, S. K.; Grimwood, D. J.; Jayatilaka, D.; Spackman, M. A. CrystalExplorer: A Program for Hirshfeld Surface Analysis, Visualization and Quantitative Analysis of Molecular Crystals. *J. Appl. Crystallogr.* **2021**, *54* (3), 1006–1011.
- (50) Liu, H.; Ye, K.; Zhang, Z.; Zhang, H. An Organic Crystal with High Elasticity at an Ultra-Low Temperature (77 K) and Shapeability at High Temperatures. *Angew. Chem. Int. Ed.* **2019**, *58* (52), 19081–19086.
- (51) Tang, S.; Ye, K.; Zhang, H. Integrating Low-Temperature-Resistant Two-Dimensional Elastic-Bending and Reconfigurable Plastic-Twisting Deformations into an Organic Crystal. *Angew. Chem. Int. Ed.* **2022**, *61* (42), e202210128.
- (52) Mahmoud Halabi, J.; Ahmed, E.; Sofela, S.; Naumov, P. Performance of Molecular Crystals in Conversion of Light to Mechanical Work. *Proc. Natl. Acad. Sci. U. S. A.* **2021**, *118* (5), e2020604118.
- (53) Tahir, I.; Ahmed, E.; Karothu, D. P.; Fschaye, F.; Mahmoud Halabi, J.; Naumov, P. Photomechanical Crystals as Light-Activated Organic Soft Microrobots. *J. Am. Chem. Soc.* **2024**, *146* (44), 30174–30182.
- (54) Yasuda, N.; Murayama, H.; Fukuyama, Y.; Kim, J.; Kimura, S.; Toriumi, K.; Tanaka, Y.; Moritomo, Y.; Kuroiwa, Y.; Kato, K.; Tanaka, H.; Takata, M. X-Ray Diffractometry for the Structure Determination of a Submicrometre Single Powder Grain. *J. Synchrotron Radiat.* **2009**, *16* (3), 352–357.
- (55) Mei, L.; An, S.-W.; Hu, K.-Q.; Wang, L.; Yu, J.-P.; Huang, Z.-W.; Kong, X.-H.; Xia, C.-Q.; Chai, Z.-F.; Shi, W.-Q. Molecular Spring-like Triple-Helix Coordination Polymers as Dual-Stress and Thermally Responsive Crystalline Metal–Organic Materials. *Angew. Chem. Int.*

*Ed.* **2020**, *59* (37), 16061–16068.

- (56) Wei, C.; Bai, L.; An, X.; Xu, M.; Liu, W.; Zhang, W.; Singh, M.; Shen, K.; Han, Y.; Sun, L.; Lin, J.; Zhao, Q.; Zhang, Y.; Yang, Y.; Yu, M.; Li, Y.; Sun, N.; Han, Y.; Xie, L.; Ou, C.; Sun, B.; Ding, X.; Xu, C.; An, Z.; Chen, R.; Ling, H.; Li, W.; Wang, J.; Huang, W. Atomic-Resolved Hierarchical Structure of Elastic  $\pi$ -Conjugated Molecular Crystal for Flexible Organic Photonics. *Chem* **2022**, *8* (5), 1427–1441.
- (57) Sheldrick, G. A Short History of SHELX. *Acta Crystallogr. A* **2008**, *64* (Pt 1), 112–122.
- (58) Kabuto, C.; Akine, S.; Nemoto, T.; Kwon, E. Release of Software (Yadokari-XG 2009) for Crystal Structure Analyses. *Nihon Kessho Gakkaishi* **2009**, *51* (3), 218–224.
- (59) Charmant, J. *Kinovea* (2023.1.2), **2024**.

TOC

### Large, rapid and continuous motion

